Analysis of global water vapour trends from satellite measurements in the visible spectral range

S. Mieruch, S. Noël, H. Bovensmann, J. P. Burrows

**Atmospheric
Chemistry
and Physics
Discussions**

**Global H$_2$O trends
from satellite
measurements**

S. Mieruch et al.

Title Page	
Abstract	Introduction
Conclusions	References
Tables	Figures
◄◄	►►
◄	►
Back	Close
Full Screen / Esc	
Printer-friendly Version	
Interactive Discussion	

EGU

Analysis of global water vapour trends from satellite measurements in the visible spectral range

S. Mieruch, S. Noël, H. Bovensmann, and J. P. Burrows

Institute of Environmental Physics, University of Bremen, FB 1, P.O. Box 330440, 28334 Bremen, Germany

Correspondence to: S. Mieruch (sebastian.mieruch@iup.physik.uni-bremen.de)

Abstract

Global water vapour total column amounts have been retrieved from spectral data provided by the Global Ozone Monitoring Experiment (GOME) flying on ERS-2, which was launched in April 1995, and the SCanning Imaging Absorption spectroMeter for Atmospheric CHartographY (SCIAMACHY) onboard ENVISAT launched in March 2002. For this purpose the Air Mass Corrected Differential Optical Absorption Spectroscopy (AMC-DOAS) approach has been used. The combination of the data from both instruments provides us with a long-term global data set spanning more than 11 years with the potential of extension up to 2020 by GOME-2 data, on Metop.

Using linear and non-linear methods from time series analysis and standard statistics the trends of H$_2$O contents and their errors have been calculated. In this study, factors affecting the trend such as the length of the time series, the magnitude of the variability of the noise, and the autocorrelation of the noise are investigated. Special emphasis has been placed on the calculation of the statistical significance of the observed trends, which reveal significant local changes of water vapour columns distributed over the whole globe.

1 Introduction

Water vapour is the most important natural greenhouse gas in the atmosphere and plays an essential role in atmospheric chemistry, e.g. the rapid conversion of sulfur trioxide to sulfuric acid, it is a source of the OH radical, and is also important for the ozone chemistry (Stenke and Grewe, 2005). In the context of climate change it plays a crucial role because of strong feedback mechanisms (Held and Soden, 2000). Thus the knowledge of the global distribution of H$_2$O and its evolution in time is of utmost importance for climatological models.

The strong infrared radiation absorbing character of H$_2$O generates the natural greenhouse effect. Without H$_2$O the global mean temperature would be 18°C lower

than today (Australian Bureau of Meteorology, 2005). The Earth's surface temperature results from an equilibrium state of the incoming solar radiation and the outgoing terrestrial radiation. Changes in the atmospheric composition, especially those of greenhouse gases such as H_2O, carbon dioxide and methane can alter the outgoing
5 terrestrial radiation which lead to a new equilibrium state between the incoming and outgoing radiation fluxes, thus resulting in a changing Earth surface temperature (Australian Bureau of Meteorology, 2005). CO_2 and CH_4, which are also measured with the SCIAMACHY instrument (Buchwitz et al., 2006), are particularly important in the discussion of the anthropogenic greenhouse effect.
10 In the debates about climate change and the greenhouse effect H_2O plays an extremely important role. For instance, climate models predict a small relative global increase of H_2O contents due to the global warming caused by increasing CO_2 and other greenhouse gases (Dai et al., 2001). This increased H_2O reduces the outgoing long-wave radiation, which yields to an additional warming of the atmosphere according
15 to Houghton et al. (2001). Together with these indirect effects on the atmospheric H_2O contents, direct influences of anthropogenic interventions such as irrigation (Boucher et al., 2004) and deforestation (Gordon et al., 2005) alter the water vapour cycle and thereby the concentrations on local as well as on global scale.

The H_2O content of the atmosphere can be seen as a proxy for the climatic state
20 of a region, whether it is, for instance, humid or dry. Moreover, it is strongly linked to the surface temperature and to the lower altitude temperature of air, respectively. This strong correlation is shown by Wagner et al. (2006). The H_2O column amounts are high over tropical rain forests, low over deserts or over the poles and medium over the temperate zone. Figure 1 shows as an example the global annual mean H_2O
25 column amounts for the year 2006 retrieved by the AMC-DOAS method (cf. Sect. 2) from SCIAMACHY data.

The H_2O trends can be seen as tracers following the climatic state of a specific region. Four different schematical scenarios of the evolution of H_2O trends can be envisaged, and are shown in Fig. 2.

Global H_2O trends from satellite measurements

S. Mieruch et al.

Full Screen / Esc

Printer-friendly Version

Interactive Discussion

EGU

These scenarios comprise

1. Top left: No trend observation, which means no change for the climatic state of the region.

2. Top right: A decreasing trend, i.e. the change from a humid state to a dry state. An infinite decreasing trend is impossible, so the trend has to stagnate at a certain point. The H_2O contents have significantly changed which could have dramatic consequences for the flora (major vegetation types, savanna, tundra etc. as reported by Melillo, 1999), fauna, agriculture and therefore inescapably for men. Moreover this new state could be stable and a way back is perhaps not easy, or, connected with a strong hysteresis (Scheffer and Carpenter, 2003).

3. Bottom left: The same as in the top right panel vice versa. Here an increasing trend pushes the system from a dry state to a humid state. As discussed above, the consequences could be profound for an ecosystem, if its exposed to such drastic changes.

4. Bottom right: The last scenario presents in principle an alternation of decreasing and increasing trends which manifests in a long-term oscillation. It is imaginable that an ecosystem can live with such an oscillation if the amplitude is not too strong and the period short enough, otherwise it will generate changes of the ecosystem.

The above schematical scenarios of the evolution of H_2O time series reveal the importance of trend detection. The H_2O contents and their changes are strongly linked to the climatic state and the vegetation type of a region. Plants, animals and humans are adapted to their environmental conditions. Changes or trends of the atmospheric H_2O amounts, e.g. to dryer or more wet situations, can have critical consequences for life. Moreover, H_2O trend calculations are important to prove model results and increase our knowledge of the hydrological cycle on global and local scale. The understanding of

H_2O correlated atmospheric processes, (e.g. evaporation, precipitation and cloud distribution) is constrained by our study. Concerning natural hazards, especially extreme rainfalls, H_2O data arises a potential early warning for possible catastrophic events. Kerr (2006) has detected such signals, which caused strong precipitation, floods and landslides. These observed H_2O patterns were firstly investigated by Zhu and Newell (1998) and called "rivers in the sky". Changes in H_2O contents, on a more local scale, could reveal the formation of such "rivers in the sky" and should be a part of a future flood forecasting system.

The importance and usefulness of H_2O trends is enormous, but the detection of such trends is difficult. The trends are influenced by several kinds of effects. First, the retrieved H_2O columns, are influenced by e.g. the surface albedo and elevation and secondly, the formulation of the trend model. On the one hand the data can be influenced by instrumental change and on the other hand natural effects such as autocorrelation in the data have to be considered. Another important natural phenomenon influencing the H_2O contents is the ENSO (El Niño Southern Oscillation). El Niño is a natural recurring (without a constant period) climate phenomenon mostly (but not solely) impacting the tropics. With respect to atmospheric H_2O the connection is performed through increasing and decreasing (depending on geolocation) surface temperatures, which cause increase and decrease of evaporation. The influence of the large El Niño event in 1997/1998 on the H_2O amounts is shown in Wagner et al. (2005). After the strong 1997/1998 El Niño, two small El Niño events took place in 2002 and 2006. Figure 3 shows the sea surface temperature (SST) anomalies (red) and the H_2O total column anomalies (blue) for the area from 4° N to 4° S and 150° W to 90° W, which are both smoothed by a 5 months running mean filter. The El Ni no event in 1997/1998 exceeds the other events by a factor of about 3. This strong coupling of the near-surface temperature anomalies with the H_2O total column anomalies is also shown in Wagner et al. (2006).

Our H_2O trend study comprises the years 1996 to 2006, i.e. 11 years of global satellite data. This length of data cannot resolve long-term oscillation as described in the

EGU

bottom right panel of Fig. 2. However, it is enough to yield significant H_2O changes on several regions on Earth.

An overview on the H_2O retrieval method and validation efforts is given in the following Sect. 2.

5   In Sect. 3 requirements for the combination of the two data sets are discussed, which are implemented in Sect. 4, where we describe the trend estimation including the statistical modelling of the time series.

Section 5 shows the results from the global trend analysis for the combined data set, and the influence of the 1997/98 El Niño event on the trends is investigated.

10 **2   Data analysis**

The global H_2O total column amounts used in the present study have been retrieved by the Air Mass Corrected Differential Optical Absorption Spectroscopy approach (AMC-DOAS) (Noël et al., 2004) from spectral data measured by the Global Ozone Monitoring Experiment (GOME) flying on ERS-2 which was launched in April 1995 and the SCan-
15 ning Imaging Absorption spectroMeter for Atmospheric CHartographY (SCIAMACHY) onboard ENVISAT launched in March 2002. The basic principle of the method is to calculate the difference between the measured Earthshine radiance and the solar irradiance at wavelengths where H_2O absorbs radiation (here we use the wavelength band from 688 nm to 700 nm) and relate this absorption-depth to the H_2O column concentra-
20 tion. The AMC-DOAS method provides a completely independent data set, because it does not rely on any additional external information. The retrieval of H_2O data from the GOME instrument is described in Noël et al. (1999), where also validation results of the data with SSM/I (Special Sensor Microwave Imager) data are shown. Likewise, SCIA-MACHY H_2O data have been validated with SSM/I and ECMWF (European Centre for
25 Medium-Range Weather Forecasts) data (Noël et al., 2005). An intercomparison and a preliminary connection of both, the GOME and the SCIAMACHY data sets, is shown in Noël et al. (2006). The high quality of the two H_2O data sets is demonstrated from

Global H_2O trends from satellite measurements

S. Mieruch et al.

Full Screen / Esc

Printer-friendly Version

Interactive Discussion

EGU

validation and comparison results, and show that they can be merged well together, thus, the trend analysis presented in this paper is build on a solid fundament. A good overview of other H_2O measuring instruments from space can be found in Brocard (2006). Previous investigations of other H_2O retrievals from GOME are described e.g. in Maurellis et al. (2000) and Lang et al. (2003). A similar H_2O trend study to ours is presented by Wagner et al. (2006) for the GOME data, based on a different retrieval method described in Wagner et al. (2003). In this study we extend the data set with the SCIAMACHY measurements and concentrate on the definition and calculation of statistically significant trends.

3 The combination of GOME and SCIAMACHY data

GOME on ERS-2 has been making measurements since June 1995 up to the present, but since June 2003 no global coverage is provided as a result of a breakdown of the on-board tape recorders. SCIAMACHY data are available since August 2002, but the SCIAMACHY instrument did not achieve final flight conditions until January 2003. The quality of the SCIAMACHY H_2O data is furthermore slightly reduced in 2002, because of the non-availability of one of the diffuser plates for solar observation prior November 2002. Overall the most appropriate time for the change from GOME to SCIAMACHY data results in 1 January 2003.

The period of near simultaneous global measurements of GOME and SCIAMACHY, August 2002 to June 2003 has been studied explicitly. The global agreement results in an average deviation of -0.01 g/cm^2 with a scatter of ± 0.25 g/cm^2 (Noël et al., 2007[1]) When producing a combined GOME/SCIAMACHY data record the following have to be taken into consideration:

---

[1]Noël, S., Mieruch, S., Bovensmann, H., and Burrows, J. P.: A combined GOME and SCIA-MACHY global H_2O data set, in: ENVISAT Symposium 2007, SP_636_ENVISAT, ESA Publications Devision, Noordwijk, The Netherlands, submitted, 2007.

EGU

1. Different equator crossing time.
    GOME on ERS-2 and SCIAMACHY onboard ENVISAT, respectively, cross the equator at 10:30 and 10:00 local time. That means SCIAMACHY and GOME measure at different times slightly different states of atmospheric composition.
    ₅ Therefore a possible mean level shift between both data sets has to be allowed for the combination of the data.

2. Differing spatial resolutions.
    The spatial resolution of the GOME data is typically 40 km×320 km, whereas it is 30 km×60 km for SCIAMACHY data. When combining both data sets, different
    ₁₀ (higher) seasonal amplitudes have to be accounted for the SCIAMACHY data with respect to GOME,

The daily H$_2$O columns are gridded on a $0.5°×0.5°$ lattice and averaged to yield monthly mean H$_2$O columns.

The H$_2$O columns are retrieved on a daily basis, but it has to be noted that ERS-2
₁₅ and ENVISAT fly on a sun-fixed orbit, i.e. passing each point on Earth at constant local time. Thus measurements from GOME and SCIAMACHY are snap-shots of the actual atmospheric conditions at specific locations at specific times.

A global coverage is achieved for GOME data within 3 days and for SCIAMACHY nadir measurements within 6 days. Thus, in principle monthly mean data provide a
₂₀ data set without gaps. However, few gaps are observed even in the monthly mean data, because high cloudiness and high mountain area (e.g. the Himalayas) measurements are removed from the data by the AMC-DOAS algorithm. Moreover, since GOME and SCIAMACHY are spectrometers using the sunlight, measurements are only possible during daylight, and therefore no data is available at night, which results in a lack of
₂₅ measurements at the poles during the polar night.

The derivation of H$_2$O columns from GOME-type instruments has also some unique advantages. The retrieval is possible over land and ocean and no external calibration sources like radiosondes are required. Moreover, looking forward to the series of

EGU

GOME-2 instruments on Metop, which result in a 25 years comprising data record.

4 Methods

4.1 Trend estimation

The detection of trends is difficult and depends on the length of the time series, the magnitude of variability and autocorrelation of the data (Weatherhead et al., 1998). The trends can be influenced by level shifts inside the time series from instrument changes or, new instrumental calibration etc.. Short time series as well as high variability, autocorrelation and level shifts in the data increase the uncertainty of trend detection. Statistical methods are used to reveal trends and explore their uncertainties. The methods used here are based on the approach of Weatherhead et al. (1998) and Tiao et al. (1990) and have been adapted to our requirements.

4.2 Statistical modelling

The time series of the data at one geolocation (i.e. a single grid point) can be described by the following trend model:

$$Y_t = \mu C_t + S_t + \omega X_t + \delta U_t + N_t, \qquad t = 0,...,T, \tag{1}$$

where Y_t contains the monthly mean H$_2$O measurements. μ is the mean water vapour content of the time series at time $t=0$ and C_t is a constant, which is unity for all t. ω represents the trend and X_t contains the time (in our case from January 1996 until December 2006 or from month 0 to 131, respectively), which is not necessarily equidistant as there may be missing data. δ is the magnitude of a mean level shift at time $t=T_0$ ($0<T_0<T$), where $T_0=84$ represents the intersection of GOME and SCIAMACHY data on January 1st 2003. U_t describes a step function:

$$U_t = \begin{cases} 0, & t < T_0 \\ 1, & t \geq T_0 \end{cases}, \tag{2}$$

Global H$_2$O trends from satellite measurements

S. Mieruch et al.

EGU

and the seasonal component S_t is modelled by a Fourier series

$$S_t = \eta \sum_{j=1}^{4} \left[\beta_{1,j} \cdot \sin(2\pi j t / 12) + \beta_{2,j} \cdot \cos(2\pi j t / 12) \right] . \qquad (3)$$

In contrast to Weatherhead et al. (1998) an additional term $\eta=1+(\gamma-1)U_t$ is used and describes an amplitude change of magnitude γ at time $t{\geq}T_0$.

⁵   The last term N_t in Eq. (1) contains the unexplained portion of the data, i.e. the noise. The noise N_t is assumed to be an autoregressive process of the order of 1 [AR(1)] (Schlittgen and Streitberg, 1997), i.e.

$$N_t = \phi N_{t-1} + \epsilon_t , \qquad (4)$$

where ϵ_t are independent random variables with zero-mean and variance σ_ϵ^2. This
¹⁰ assumption is used because environmental data is often autocorrelated, e.g. if the temperature is high at one day, a high temperature is probably on the next day. The magnitude or the memory of the autocorrelation is presented by ϕ, which is restricted to $-1<\phi<1$, so the noise process N_t is stationary. The memory of the data at lag one can be calculated using the autocorrelation function $\phi=\mathrm{Corr}_{N_t N_{t-1}}$, which is directly linked
¹⁵ to the well known correlation coefficient. More sophisticated approaches of analysing long-term correlations in environmental data are the Detrended Fluctuation Analysis (DFA) (Rybski et al., 2006) and the modelling of time series with Markov-Chains (Freund et al., 2006). However, we are interested in the autocorrelation at lag one, thus the autocorrelation function is adequate for our purposes.

²⁰   Generally the autocorrelation function is restricted to continuous, statistically stationary stochastic functions, or in the discrete case equidistantly sampled data. Since there are gaps in our time series the discrete correlation function for analysing unevenly sampled data which was originally developed by Edelson and Krolik (1988) for astronomical problems, was applied.

²⁵   To calculate the autocorrelation of the noise, the noise itself has to be determined by applying the model (Eq. 1) to the data and subtract the fit from the data. For minimis-

ing the model in a least square sense we used the well known Levenberg-Marquardt algorithm for non-linear least square regression. The noise N_t is then given by the remaining residuals:

$$N_t = Y_t - (\hat{\mu}C_t + \hat{S}_t + \hat{\omega}X_t + \hat{\delta}U_t) \,, \tag{5}$$

where $\hat{\mu}$, $\hat{\omega}$, $\hat{\delta}$ are the least square estimators and $\hat{S}_t$ stands for the seasonal component resulting from the fitted parameters $\hat{\beta}_{i,j}$ and $\hat{\gamma}$. The N_t are used to calculate first the set of unbinned discrete correlations

$$\theta_t = \frac{N_t \cdot N_{t-1}}{\sigma_N^2} \,, \qquad t = 1,...,T \,, \tag{6}$$

where the N_t have zero-mean and variance σ_N^2. Following the θ_t have to be assigned to their lags, τ_t with

$$\tau_t = X_t - X_{t-1} \,, \qquad t = 1,...,T \,. \tag{7}$$

Now, the magnitude ϕ of autocorrelation at lag $\tau=1$ can be determined by averaging over the number M of θ_t with corresponding $\tau_t=1$:

$$\phi = \frac{1}{M} \sum_{i=1}^{M} \theta_i(\tau_i = 1) \,. \tag{8}$$

The great benefit of the discrete correlation function is that we can calculate a standard deviation

$$\sigma_\phi = \sqrt{\frac{1}{M-1} \sum_{i=1}^{M} (\theta_i(\tau_i = 1) - \phi)^2} \tag{9}$$

and a standard error of the mean

$$S_\phi = \frac{\sigma_\phi}{\sqrt{M}} \,. \tag{10}$$

Global H$_2$O trends from satellite measurements

S. Mieruch et al.

Title Page

Abstract | Introduction

Conclusions | References

Tables | Figures

◄ | ►

◄ | ►

Back | Close

Full Screen / Esc

Printer-friendly Version

Interactive Discussion

EGU

The aim of the above calculations concerning autocorrelations is to account for them during the fitting procedure. For this purpose the seasonal component S_t is subtracted from the data, because it has negligible effect on the estimation of the other parameters (Weatherhead et al., 1998). The model then becomes

$$A_t = \mu C_t + \omega X_t + \delta U_t + N_t \,, \qquad t = 0,...,T \,. \tag{11}$$

After the non-linear terms have been removed from the model a linear matrix transformation to consider the autocorrelations is possible. Making the connection to the autoregressive process of Eq. (4), the model has absorbed the autocorrelations of N_t into the transformed data A_t^*, the constant C_t^*, the time X_t^* and the step function U_t^*, whereas the N_t have lost their autocorrelations and have become white noise e_t:

$$A_t^* = \mu C_t^* + \omega X_t^* + \delta U_t^* + \epsilon_t \,, \qquad t = 0,...,T \,. \tag{12}$$

Now a linear regression is applied, which can be solved analytically for the least square estimators $\hat{\mu}$, $\hat{\omega}$, $\hat{\delta}$ and their errors $\sigma_{\hat{\mu}}$, $\sigma_{\hat{\omega}}$, $\sigma_{\hat{\delta}}$. Details of the transformation and regression are given in the Appendix and in Weatherhead et al. (1998).

4.2.1 Trend fitting and estimation of the uncertainty

After the implementation of the autocorrelations into the model and solving the linear least square equations (where we denote the least square estimator of the trend with $\hat{\omega}$) a good approximation of the error of the trend $\sigma_{\hat{\omega}}$ is given by (Weatherhead et al., 1998):

$$\sigma_{\hat{\omega}} \approx \frac{\sqrt{12}\,\sigma_N}{\ell^{\frac{3}{2}}} \cdot \sqrt{\frac{1+\phi}{1-\phi}} \cdot \frac{1}{[1 - 3\vartheta(1-\vartheta)]^{\frac{1}{2}}} \,. \tag{13}$$

$\sigma_{\hat{\omega}}$ depends on the standard deviation σ_N of the noise, the length of the time series ℓ, the autocorrelation ϕ of N_t and the fraction $\vartheta = T_0/\ell$ of the data before the level shift occurs.

EGU

4.2.2 Significance of the trend

One main question concerning trends is whether the trend is significant or not. The answer to this question can only be given in a statistical sense talking about probabilities. Based on the null hypothesis that the observed trend is equal to zero $H_0 : \hat{\omega}=0$ the alternative hypothesis is the observation of a nonzero trend $H_1 : \hat{\omega}\neq0$. Assuming a Gaussian distribution of the trends, the probability of measuring a trend with magnitude greater than two times its error becomes $P_{H_0}\{|\hat{\omega}|>2\sigma_{\hat{\omega}}\}=0.05$ and the chance of making an error in rejecting the null hypothesis is 5 %. Accordingly, the likelihood to be correct in confiding the alternative hypothesis is 95 %. Therefore we will adopt the rule that a trend $\hat{\omega}$ is statistically significant when a probability of 95 % is achieved with $|\hat{\omega}| > 2\sigma_{\hat{\omega}}$.

5 Results

5.1 Global trend patterns

The global trend patterns are determined from the long-term time series from January 1996 to December 2006 including GOME and SCIAMACHY globally gridded monthly mean data on a 0.5°×0.5° grid. Two ways of investigating the trends are informative; on the one hand displaying the absolute trends $\hat{\omega}$ in g/cm^2 per year (Fig. 4 left) and on the other hand displaying the relative trends $\hat{\omega}/\hat{\mu}$ in % per year (Fig. 4 right), where $\hat{\mu}$ represents the deseasonalised H_2O contents at the beginning of the time series.

The absolute trends shown in Fig. 4 are stronger near the equator and smaller near the poles. Bluish as well as yellowish and reddish patches are seen, thus there are negative as well as positive trends observed, however most trends are small and distributed around zero. The relative trends in Fig. 4 provide additional information about the magnitude of the H_2O content at a specific site.

Now the question arises if these observed trends are significant in a statistical way. Here it has to be noted, that a non-significant trend does not mean that the results are

EGU

wrong, but that the magnitude of the observed trend has a higher uncertainty. We will use the significance definition from Sect. 4.2.2 that a trend is significant if it is greater than two times its error (Weatherhead et al., 1998). In addition we will extend the significance criterion by the claim, that the time series has to contain at minimum 2/3 of the maximum data points and denote this additional criterion with $\ell \geq 2/3L$, where ℓ is the number of data points of a specific time series and L is the number of maximum data points. In our case we have 11 years of monthly data, yielding $L=132$ and $\ell \geq 88$. Figure 5 shows the significant trends (left absolute, right relative), which are distributed over the whole globe. The significant trends agree with either strong absolute or strong relative trends. However, it is interesting that also small absolute (e.g. Antarctica) or small relative trends (e.g. Amazonia) can be significant.

Figure 5 reveals several local regions with significant trends, for instance increasing H_2O contents in Greenland, East Europe, Siberia and Oceania. Water vapour decrease is observed in the northwest USA, Central America, Amazonia, Central Africa and the Arabian Peninsular.

Since H_2O trends are usually quite small, the consideration of both, the level shift and the amplitude change during the fit routines, is highly important, especially the level shift. Considering or not considering the level shift δ has crucial consequences for the trends. This is revealed from a trend calculation only for the GOME data, were we observed quite similar results to the combined data using the level shift. Disregarding the level shift yields rather different findings. Concluding, the integration of the level shift term (which is investigated statistically in Sect. 5.3) in our model is absolute necessary for our trend calculation.

Neglecting the change in the amplitude yields on the one hand a higher noise signal in the deseasonalised data A_t. On the other hand a remaining seasonal component is left in the N_t, which results in changing autocorrelations. Both aspects are not critical for the trends, but crucial for the estimation of the errors of the trends (Eq. 13) and therefore the significance of the trends.

[EGU]

5.2 Globally averaged monthly mean H_2O trend

Our trend analysis is applied to a time series of deseasonalised globally averaged monthly mean H_2O columns shown in Fig. 6 including the strong 1997/1998 El Niño data (left) and disregarding the 1997/1998 El Niño data (right). As can be seen from Fig. 3 the two El Niño events in 2002 and 2006 are small compared to the El Niño in 1997/1998. Here, we can benefit from the consideration of the autocorrelation, because the possible change in H_2O caused by an El Niño event changes the autocorrelation of the data. For instance increasing H_2O contents over a limiting time increase the autocorrelation which yields to a higher error $\sigma_{\hat{\omega}}$ of the trend, because autocorrelations are considered in Eqs. (12) and (13). Hence it is not necessary to remove small events such as 2002 and 2006.

It has to be noted that a weighted mean is used when accumulating spatial measurements on a regular latitude/longitude grid, where the weights are given by the cosine of the latitude of each grid point, to account for the different surface areas. The red line, corresponding to the fit parameter $\hat{\omega}$, in the left panel of Fig. 6 shows an increase of $0.0029\,\mathrm{g/cm^2}\pm0.0028\,\mathrm{g/cm^2}$ per year, i.e. 0.14 % per year related to the fitted parameter $\hat{\mu}=2.03\,\mathrm{g/cm^2}$. This trend is non-significant, because the high autocorrelation of $\hat{\phi}=0.6$ increases the error of the trend $\sigma_{\hat{\omega}}$ as can be seen from Eq. (13).

One reason for the high autocorrelation is the presence of high H_2O column amounts around the year 1998, which are most likely caused by the El Niño event. These higher columns are also reported by Wagner et al. (2005) for H_2O retrieved from GOME data by a different algorithm.

As stated above the 1997/1998 El Niño event is most likely influencing the trend in the left panel of Fig. 6, and probably data obtained during the El Niño time have to be removed as a kind of recurring phenomenon. Otherwise it is not clear if El Niño can be totally separated from the trend, because it cannot be excluded that for instance due to an increasing H_2O trend the magnitude of the El Niño is increased. Nevertheless, we identify the strong 1997/1998 El Niño in the time series and remove the corresponding

EGU

data to quantify the effect on the trends, especially on the significance of the trends. The influence of the 1997/1998 El Niño is shown in Fig. 7, where the months are plotted against the years and the globally averaged deseasonalised H_2O column amounts are coded with colours.

As can be seen from Fig. 7, high H_2O contents are observed from September 1997 until March 1999. Accordingly, the global trend analysis is performed again with the data set where we removed these potentially El Niño influenced data. The differences on the global map between the complete data and the data where we removed El Niño is quite small and also the significant trends are almost similar. This can be explained by the fact, that as a result of the autocorrelation correction the influence of El Niño is reduced, i.e. data which is strongly influenced by El Niño is mostly non-significant, because of high errors of the trend.

The right plot of Fig. 6 depicts the deseasonalised spatially averaged monthly mean column amounts for the data with the El Niño event removed.

The trend (red line) yields $0.0039\,g/cm^2 \pm 0.0015\,g/cm^2$ per year or 0.20 % per year thus the trend is significant with $\hat{\omega} > 2.6\sigma_{\hat{\omega}}$. The magnitude of the level shift is increased with respect to the level shift in the left panel. The reason therefore is that the autocorrelation of the time series is decreased to $\hat{\phi} = 0.2$ and affects the fit parameters much less without the El Niño data. Hence, there is a strong contribution of the 1997/1998 El Niño event to the autocorrelations of the time series.

To demonstrate the sensitivity of the calculated trends ω and their errors σ_{ω} to the used regression model and data set, several fitting procedures are performed for the single time series of deseasonalised globally averaged monthly mean data. The trend estimation (shown in Table 1) is applied, with and without the 1997/1998 El Niño data, to GOME (January 1996 to December 2002) measurements only and to the complete data set based on GOME and SCIAMACHY measurements (January 1996 to December 2006). The first column of Table 1 indicates the fitting method used, i.e. all permutations of considering and neglecting (denoted as cancelled parameter) the level shift δ and the autocorrelation ϕ of the noise N_t.

Global H_2O trends from satellite measurements

S. Mieruch et al.

Title Page

Abstract	Introduction
Conclusions	References
Tables	Figures

◄ | ►|

◄ | ►

Back | Close

Full Screen / Esc

Printer-friendly Version

Interactive Discussion

As can be seen from Table 1, fitting a single H_2O time series (in this case the global monthly mean data) is quite sensitive to the regression model used. Applying the full model used in this paper (considering δ and ϕ) delivers the most reliable results, which is explained below:

[δ , ϕ]: Both parameters, the level shift and the autocorrelation, are fitted to the complete data set. Including El Niño yields the trend from the left panel of Fig. 6, which is relatively high, because the consideration of ϕ attenuates the high H_2O measurements in 1997/98. Otherwise a high error is observed, because fitting δ and ϕ introduces additional uncertainties and therefore increases the error (cf. Eq. 13). Neglecting El Niño increases the trend and decreases the error, because the resulting data contains less autocorrelations and less noise.

[δ , $\cancel{\phi}$]: The trend calculation is performed without regarding autocorrelations with the consequence that the high H_2O amounts in 1997/98 lift up the trend curve at that time and the magnitude of the trend is nearly zero. Furthermore the error is decreased, because no autocorrelation is considered. However, the relative error is still about 100 %. If the El Niño data is masked the trend and its error have hardly changed compared to the "full fit", because ϕ is quite small without El Niño data.

[$\cancel{\delta}$, ϕ]: Fitting only the GOME time series from January 1996 to December 2002 and including autocorrelations yields an almost zero trend, because of the strong influence of El Niño in 1997/98. On the contrary, if the El Niño data is removed, the trend and its error is quite similar to those calculated for the complete data considering both parameters. If the regression without δ is performed for the complete data set, the trend is increased, which is clear, because a positive level shift (see Fig. 6), which exists but is not fitted, increases the trend. When the El Niño data is removed the level shift is even larger, which can be seen in Fig. 6. In this case neglecting the level shift strongly increases the trend.

Global H_2O trends from satellite measurements

S. Mieruch et al.

Title Page

Abstract	Introduction
Conclusions	References
Tables	Figures

◄◄ ►►

◄ ►

Back Close

Full Screen / Esc

Printer-friendly Version

Interactive Discussion

EGU

[δ, ϕ]: Neglecting autocorrelations results for the GOME data with El Niño in a nearly zero slightly negative trend, whereas without El Niño the trend is quite high as in the case above. For the complete GOME and SCIAMACHY data the situation is similar to the above scenario. The negligence of δ extremely influences the trend.

Concluding the analysis of the consideration or negligence of the level shift and the autocorrelations with respect to different data sets reveal that the full method applied to the complete data set (as used in this paper) is the most reliable approach. The complete time series therefore has to be used for the trend estimation. If the 1997/1998 El Niño data is neglected, the trends are significant, with respect to our criterion $|\omega| > 2\sigma_\omega$. A distinct agreement is observed for the trends calculated from the GOME data and the complete data with removed El Niño, but considered level shift δ. In contrast, the trends from the GOME data disagree with the trends from the complete set neglecting the level shift. Therefore the consideration of the level shift is necessary, because an increase of the trends from the GOME set to the complete set by a factor of about two is most unlikely. Also the trends including El Niño data from the complete data set (using the level shift) and the GOME data agree within their errors, whereas the negligence of the level shift strongly increases the trends, which is most probably wrong. The consideration of the autocorrelations is necessary when the El Niño data is included. Removing the El Niño data decreases the importance of the autocorrelation, however there is still autocorrelation in the data which has to be eliminated.

5.3 Influence of the level shift and the amplitude change

The above analysis showed that the derived trends are significantly affected by the level shift. Therefore we present the results of a statistical investigation of the fitted level shift δ and also the amplitude change γ and reveal their distributions. A statistical analysis of the least square estimator $\hat{\delta}$ of the mean level shift is shown in the left panel of Fig. 8 were the density distribution (red bars) with binsize 0.02 g/cm^2 of the $\hat{\delta}$ for the

whole globe is plotted. The black line denoted with G describes a Gaussian which is fitted to the distribution of the $\hat{\delta}$.

The level shifts between GOME and SCIAMACHY data reveal a slightly narrower distributed offset than a Gaussian normal distribution between both instruments. A description in terms of quantiles is quite suitable. The 10 % quantile, denoted as Q10 (magenta line) in Fig. 8 in the left panel, lies at −0.096 g/cm^2, the 50 % quantile (the median blue line) has a magnitude of Q50=0.005 g/cm^2 and the 90 % quantile (cyan line) is observed at Q90=0.162 g/cm^2. Strictly speaking, in most cases the H_2O columns do not change, which is reflected by the nearly zero median, but with a probability of 10 % it changes less than −0.096 g/cm^2 and more than 0.162 g/cm^2 (also with a probability of 10 %), which corresponds to −4.7 % and 8.0 %, respectively, related to the global mean H_2O content at the beginning of the time series (fitted parameter μ) of about 2.03 g/cm^2. This scatter of the level shift is attributed to the time delay between the two instruments as well as to the high variability of atmospheric H_2O. Most likely also cloud statistics play a crucial role, because no H_2O measurements at locations with thick cloud covers are possible.

The right panel of Fig. 8 depicts the global density distribution (binsize 0.02) of the amplitude changes $\hat{\gamma}$ together with a fitted Gaussian (black curve) denoted by G. As expected, as a result of the higher resolution of the SCIAMACHY instrument, the amplitude factors $\hat{\gamma}$ are higher than one with a median of Q50=1.029 (blue line), but with a scatter of Q10=0.852 (magenta line) and Q90=1.232 (cyan line). From this analysis, it is clear that the natural variability of H_2O dominates the changing amplitude. In addition the cloud statistics, i.e. the amount and distribution of clouds may be impacting on the amplitude.

Concluding, both the mean level shift and the amplitude change at the intersection of the GOME and SCIAMACHY data are small compared to the H_2O column amounts. However they need to be considered in the trend analysis, because the observed trends are also small.

EGU

6 Conclusions and discussion

The trend analysis (of global monthly mean H_2O data from 1996 to 2006) focussed on the estimation of the statistical significance of the observed trends. First the trends were calculated from monthly mean H_2O column amounts where we removed the seasonal component. Special emphasis was placed on the consideration of autocorrelations in the data. The trend calculation, which is based on the well known least square linear regression, provides an error for the trend. This error is influenced by the length of the time series, the noise, the autocorrelation of the noise, and the level shift between GOME and SCIAMACHY data.

Two criteria for a significant trend are proposed:

(a) A trend has to be greater than 2 times its error, which arises from standard statistics.

(b) The time series has to comprise minimum 2/3 of the maximum data, which is required as a quality criterion.

For the period of January 1996 to December 2006 we found significant increase in the H_2O amounts (cf. Fig. 5) in Greenland, East Europe, Siberia and Oceania, and we have significant decrease in the northwest USA, Central America, Amazonia, Central Africa, and the Arabian Peninsular. Following the schematic scenarios from Fig. 2, the significant trends can be interpreted as tracers of the climatic state, hence these regions are changing their states, e.g. from dry to humid (scenario 2) or from moist to dry (scenario 3). However long-term oscillations (scenario 4) cannot be excluded.

For the whole globe the increasing trend is non-significant when taking into account the 1997/1998 El Niño event, which is seen in the globally averaged data as strong positive H_2O amounts from September 1997 to March 1999. Masking the El Niño time span we find a significant H_2O trend of $0.0039\,g/cm^2 \pm 0.0015\,g/cm^2$ per year or 0.20 % per year. Even stronger trends up to 5 % per year are observed on local scales.

Title Page

Abstract | Introduction

Conclusions | References

Tables | Figures

|◄ | ►|

◄ | ►

Back | Close

Full Screen / Esc

Printer-friendly Version

Interactive Discussion

[EGU]

The H_2O content is changing and the human impact on this is not clear. Though the anthropogenic intervention in nature is beyond all question, on the one hand humans irrigate fields (which has a direct effect on the atmospheric H_2O contents reported by Boucher et al., 2004) for agriculture, on the other hand they drain swamps. Woods are deforested and grassland is concreted. Diamond (2005) refers to drastic anthropogenic interventions such as deforestation and high consumption of groundwater in the northwest USA (especially in Montana), where we detect significant H_2O decrease. For instance Gordon et al. (2005) attribute a decrease in H_2O flow of the Brazilian Amazon region to 15 % deforested rainforest, which is in line with our observed decreasing trends.

At present the contribution of natural and anthropogenic induced changes remains unclear.

A planned work is a correlation analysis between our H_2O data set and cloud data, surface temperature data and other meteorological measurements for instance surface albedo values and precipitation. Especially important is the investigation of cloud data because it will contribute to a better understanding of the H_2O data, because of their strong coupling. As stated above human activities alter the land cover on Earth. Therefore data sets which are directly linked to anthropogenic interventions such as irrigation and deforestation can be very helpful to distinguish between humanly caused changes and natural alterations. The influence of the El Niño event on the trends, which can be seen in our data, is an interesting point and needs further investigation.

From Fig. 2 one can imagine that at a certain length of the time series a linear regression is not suitable, i.e. when there is more than one trend in the time series. Dose and Menzel (2006) describe how a changing trend over time can be estimated for long-term time series, which could be a useful method for the analysis of the extended data set comprising GOME, SCIAMACHY and GOME-2 (on Metop) measurements.

Global H$_2$O trends from satellite measurements

S. Mieruch et al.

[EGU](#)

Appendix A

Trend fitting and estimation of the uncertainty

The following steps show the calculating of the trend ϖ and the uncertainty of the trend
σ_ϖ regarding autocorrelations. Equation (11) can be cast into compact matrix notation

$$A = \mathbf{X}\beta + N \, , \tag{A1}$$

where A is the $\ell \times 1$ vector of observation, $\mathbf{X}$ is a $\ell \times 3$ matrix consisting of the constant C_t, time X_t and step function U_t. $\beta = (\mu, \varpi, \delta)'$ represents the vector of unknown regression coefficients and N is the noise vector afflicted with autocorrelations.

The N_t are directly calculated from the time series (cf. Eq. 5) and with the connection to the ϵ_t from Eq. (4) only the ϵ_t for $t = 1, \dots, T$ can be calculated via

$$\epsilon_t = N_t - \phi N_{t-1} \tag{A2}$$

because no N_{-1} exists. Therefore the ϵ_0 has to be estimated by $\epsilon_0 = \sqrt{1 - \phi^2} N_0$ which is motivated by the assumption

$$\frac{\sigma_\epsilon}{\sigma_N} \approx \frac{\epsilon_t}{N_t} \, . \tag{A3}$$

A matrix $\mathbf{P}'$ is constructed which satisfies:

$$\mathbf{P}' N = \epsilon \tag{A4}$$

which is in detail:

$$\begin{pmatrix} \sqrt{1 - \phi^2} & 0 & 0 & \dots \\ -\phi & 1 & 0 & \dots \\ 0 & -\phi & 1 & \dots \\ \vdots & & \vdots & \vdots & \vdots \end{pmatrix} \cdot \begin{pmatrix} N_0 \\ N_1 \\ N_2 \\ \vdots \end{pmatrix} = \begin{pmatrix} \epsilon_0 \\ \epsilon_1 \\ \epsilon_2 \\ \vdots \end{pmatrix} \tag{A5}$$

Title Page

Abstract | Introduction

Conclusions | References

Tables | Figures

◄ | ►

◄ | ►

Back | Close

Full Screen / Esc

Printer-friendly Version

Interactive Discussion

EGU

so that $N = P'^{-1}\epsilon$.

The model Eq. (A1) becomes:

$$A = X\beta + P'^{-1}\epsilon . \tag{A6}$$

Using matrix algebra, the model can be written as

$$P'A = P'X\beta + \epsilon \tag{A7}$$

or using the transformed variables $A^* = P'A$ and $X^* = P'X$ we have

$$A^* = X^*\beta + \epsilon . \tag{A8}$$

Now we have absorbed the autocorrelations in the transformed variables A^* and X^* of model Eq. (A8) and we can apply a least square fit. The least square estimator can be calculated by:

$$\hat{\beta} = (X^{*\prime}X^*)^{-1}X^{*\prime}A^* . \tag{A9}$$

Denoting the diagonal elements of $(X^{*\prime}X^*)^{-1}$ with v_j the variance of $\hat{\beta}$ becomes:

$$\mathrm{Var}(\hat{\beta}_j) = \sigma_\epsilon^2 v_j , \qquad j = 1, 2, 3 , \tag{A10}$$

where σ_ϵ^2 stands for the variance of the ϵ_t. Therefore the variance of the trend estimator $\hat{\omega}$ is

$$\sigma_{\hat{\omega}}^2 = \mathrm{Var}(\hat{\omega}) = \sigma_\epsilon^2 v_2 . \tag{A11}$$

The variance $\sigma_{\hat{\omega}}^2$ or the standard deviation $\sigma_{\hat{\omega}}$, respectively, of the trend estimator considers the length of the data (ℓ), the contained noise (σ_ϵ), the autocorrelation of the noise (ϕ) and additionally the position of the level shift (ϑ), but not its magnitude. Thus $\sigma_{\hat{\omega}}$ can be written as

$$\sigma_{\hat{\omega}} = \frac{\sqrt{12}\,\sigma_\epsilon}{(1 - \phi)\cdot[\ell(\ell^2 - 1)]^{\frac{1}{2}}} \cdot \frac{1}{[1 - 3\vartheta(1 - \vartheta)]^{\frac{1}{2}}} , \tag{A12}$$

where $\vartheta = T_0/\ell$ is the fraction of the data before the level shift occurs. With the assumption $\ell(\ell^2-1) \approx \ell^3$ Eq. (A12) can be written as:

$$\sigma_{\hat{\omega}} \approx \frac{\sqrt{12}\,\sigma_\epsilon}{(1-\phi)\cdot\ell^{\frac{3}{2}}} \cdot \frac{1}{[1-3\vartheta(1-\vartheta)]^{\frac{1}{2}}}\ . \tag{A13}$$

The variance σ_N of the autocorrelated noise N_t is directly related to the variance σ_ϵ of the white noise ϵ_t by $\sigma_N^2 = \sigma_\epsilon^2/(1-\phi^2)$, thus a good approximation is found with

$$\sigma_{\hat{\omega}} \approx \frac{\sqrt{12}\,\sigma_N}{\ell^{\frac{3}{2}}} \cdot \sqrt{\frac{1+\phi}{1-\phi}} \cdot \frac{1}{[1-3\vartheta(1-\vartheta)]^{\frac{1}{2}}}\ . \tag{A14}$$

More details on the estimation of the trend uncertainty can be found in Tiao et al. (1990) and Weatherhead et al. (1998).

References

Australian Bureau of Meteorology, The Greenhouse Effect and Climate Change, http://www.bom.gov.au/info/GreenhouseEffectAndClimateChange.pdf, 2005. 11763

Boucher, O., Myhre, G., and Myhre, A.: Direct human influence of irrigation on atmospheric H_2O and climate, Clim. Dynam., 22, 597–603, 2004. 11763, 11781

Brocard, E.: Overview on satellite experiments which measure atmospheric water vapor. IAP Research Report, Institut für angewandte Physik, Universität Bern, Bern, Switzerland, 2006. 11767

Title Page

Abstract | Introduction

Conclusions | References

Tables | Figures

◀◀ | ▶▶

◀ | ▶

Back | Close

Full Screen / Esc

Printer-friendly Version

Interactive Discussion

EGU

Buchwitz, M., de Beek, R., Noël, S., Burrows, J. P., Bovensmann, H., Schneising, O., Khlystova, I., Bruns, M., Bremer, H., Bergamaschi, P., Körner, S., and Heimann, M.: Atmospheric carbon gases retrieved from SCIAMACHY by WFM-DOAS: version 0.5 CO and CH4 and impact of calibration improvements on CO2 retrieval, Atmos. Chem. Phys. 6, 2727–2751, 2006. 11763

Dai, A., Meehl, G. A., Washington, W. M., Wigley, T. M. L., and Arblaster, J. A.: Ensemble simulation of twenty-first century climate changes: Business-as-usual versus CO2 stabilization, B. Am. Meteorol. Soc., 82, 2377–2388, 2001. 11763

Diamond, J.: How Societies Choose to Fail or Succeed, Collaps, Viking, Penguin Group, New York, 45–99, 2005. 11781

Dose, V. and Menzel, A.: Bayesian correlation between temperature and blossom onset data, Global Change Biol., 12, 1451–1459, 2006. 11781

Edelson, R. A., Krolik, J. H.: The discrete correlation function: A new method for analyzing unevenly sampled variability data, Astrophys. J., 333, 646–659, 1988. 11770

Freund, J. A., Pöschel, T., and Wiltshire, K. H.: Markovsche Analyse nasser Gemeinschaften, Logos, Berlin, pp.99–110, 2006. 11770

Gordon, L. J., Steffen, W., Jörnsen, B. F., Folke, C., Falkenmark, M., Johannessen, Å., 2005. Human modification of global water vapor flows from the land surfaces, PNAS 102, 7612–7617, 2005. 11763, 11781

Held, I. M. and Soden, B. J.: Water Vapor Feedback And Global Warming, Annu. Rev. Energy Environ., 25, 441–75, 2000. 11762

Houghton, J. T., Ding, Y., Griggs, D. J., Noguer, M., van der Winden, P., and Dai, X.: Climate Change 2001: The Scientific Basis. Contribution of Working Group I to the Third Assessment Report, Cambridge Univ. Press, 423pp., 2001. 11763

Kerr, R. A.: Rivers in the Sky Are Flooding the World With Tropical Waters, Science 313, 435, 2006. 11765

Lang, R., Williams, J. E., van der Zande, W. J., and Maurellis, A. N.: Application of the Spectral Structure Parameterization technique: retrieval of total water vapor columns from GOME, Atmos. Chem. Phys. 3, 145–160, 2003. 11767

Maurellis, A. N., Lang, R., van der Zande, W. J., Aben, I., and Ubachs, W.: Precipitable water vapor column retrieval from GOME data, Geophys. Res. Lett., 27(6), 903–906, 2000. 11767

Melillo, J. M.: Climate Change: Warm, Warm on the Range, Science, 8, 183–184, 1999. 11764

Noël, S., Buchwitz, M., Bovensmann, H., Hoogen, R., and Burrows, J. P.: Atmospheric Water

Title Page

Abstract | Introduction

Conclusions | References

Tables | Figures

|◄ | ►|

◄ | ►

Back | Close

Full Screen / Esc

Printer-friendly Version

Interactive Discussion

EGU

Vapor Amounts Retrieved from GOME Satellite Data, Geophys. Res. Lett., 26(13), 1841–1844, 1999. 11766

Noël, S., Buchwitz, M., and Burrows, J. P.: First retrieval of global water vapour column amounts from SCIAMACHY measurements, Atmos. Chem. Phys. 4, 111–125, 2004. 11766

Noël, S., Buchwitz, M., Bovensmann, H., and Burrows, J. P.: Validation of SCIAMACHY AMC-DOAS H_2O columns, Atmos. Chem. Phys. 5, 1835–1841, 2005. 11766

Noël, S., Mieruch, S., Buchwitz, M., Bovensmann, H., and Burrows, J. P.: GOME and SCIA-MACHY global H_2O columns, in: Proceedings of the First Atmospheric Science Conference, ESA Publications Desision, Noordwijk, The Netherlands, http://earth.esa.int/cgi-bin/confatmos06.pl?abstract=166, 2006. 11766

Rybski, D., Bunde, A., Havlin, S., and von Storch, H.: Long-term persistence in climate and the detection problem, Geophys. Res. Lett., 33, LO3718, doi:10.1029/2005GL025591, 2006. 11770

Scheffer, M. and Carpenter, S. R.: Catastrophic regime shifts in ecosystems: linking theory to observation, Trends Ecol. Evol., 18, 648–656, 2003. 11764

Schlittgen, R. and Streitberg, B. H. J.: Zeitreihenanalyse, Oldenbourg, München, 1997. 11770

Stenke, A. and Grewe, V.: Simulation of stratospheric water vapor trends: impact on stratospheric ozone chemistry, Atmos. Chem. Phys., 5, 1257–1272, 2005, http://www.atmos-chem-phys.net/5/1257/2005/. 11762

Tiao, G. C., Reinsel, G. C., Xu, D., Pedrick, J. H., Zhu, X., Miller, A. J., DeLuisi, J. J., Mateer, C. L., and Wuebbles, D. J.: Effects of autocorrelation and temporal sampling schemes on estimation of trend and spatial correlation, J. Geophys. Res., 95, 20 507–20 517, 1990. 11769, 11784

Wagner, T., Heland, J., Zöger, M., and Platt, U.: A fast H_2O total column density product from GOME – Validation with in-situ aircraft measurements, Atmos. Chem. Phys., 3, 651–663, 2003, http://www.atmos-chem-phys.net/3/651/2003/. 11767

Wagner, T., Beirle, S., Grzegorski, M., Sanghavi, S., and Platt, U.: El Niño induced anomalies in global data sets of total column precipitable water and cloud cover derived from GOME on ERS-2, J. Geophys. Res., 110, D15104, doi:10.1029/2005JD005972, 2005. 11765, 11775

Wagner, T., Beirle, S., Grzegorski, M., and Platt, U.: Global trends (1996–2003) of total column precipitable water observed by Global Ozone Monitoring Experiment (GOME on ERS-2) and their relation to near-surface temperature, J. Geophys. Res., 111, D12102,

Title Page

Abstract | Introduction

Conclusions | References

Tables | Figures

◄ | ►

◄ | ►

Back | Close

Full Screen / Esc

Printer-friendly Version

Interactive Discussion

EGU

doi:10.1029/2005JD006523, 2006. 11763, 11765, 11767

Weatherhead, E. C., Reinsel, G. C., Tiao, G. C., Meng, X.-L., Choi, D., Cheang, W.-K., Keller, T., DeLuisi, J., Wuebbles, D. J., Kerr, J. B., Miller, A. J., Oltmans, S. J., Frederick, J. E.: Factors affecting the detection of trends: Statistical considerations and applications to environmental data, J. Geophys. Res., 103, 17 149–17 161, 1998. 11769, 11770, 11772, 11774, 11784

Zhu, Y. and Newell, R. E.: A Proposed Algorithm for Moisture Fluxes from Atmospheric Rivers, Mon. Wea. Rev., 126, 725–735, 1998.
11765

Title Page

Abstract | Introduction

Conclusions | References

Tables | Figures

◄ | ►

◄ | ►

Back | Close

Full Screen / Esc

Printer-friendly Version

Interactive Discussion

EGU

EGU

Table 1. Results from several fitting procedures show the sensitivity of the trends ω and their errors σ_ω (in g/cm^2 per year) to the consideration of the level shift δ and the autocorrelations ϕ.

	including El Niño data		neglecting El Niño data	
	GOME	GOME & SCIA	GOME	GOME & SCIA
δ , ϕ	–	0.0029 ± 0.0028	–	0.0039 ± 0.0015
δ , $\cancel{\phi}$	–	0.0002 ± 0.0002	–	0.0037 ± 0.0012
$\cancel{\delta}$, ϕ	0.0006 ± 0.0040	0.0043 ± 0.0019	0.0034 ± 0.0015	0.0072 ± 0.0010
$\cancel{\delta}$, $\cancel{\phi}$	−0.0010 ± 0.0019	0.0041 ± 0.0009	0.0033 ± 0.0012	0.0073 ± 0.0007

EGU

2006

H$_2$O vertical column amounts in g/cm^2
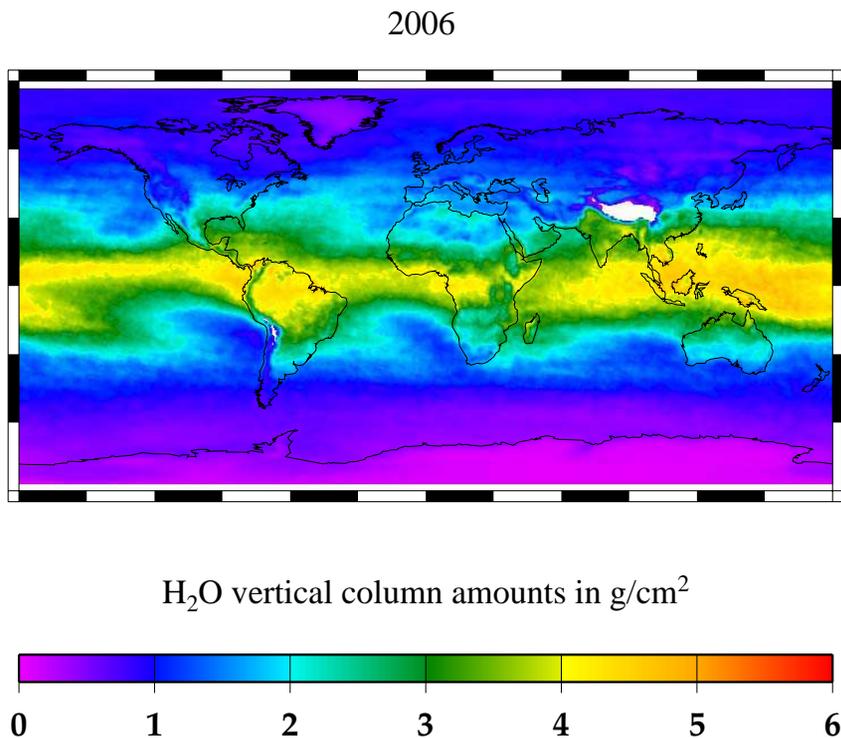
Fig. 1. Annual mean H$_2$O column amounts for the year 2006 derived from SCIAMACHY measurements.

EGU
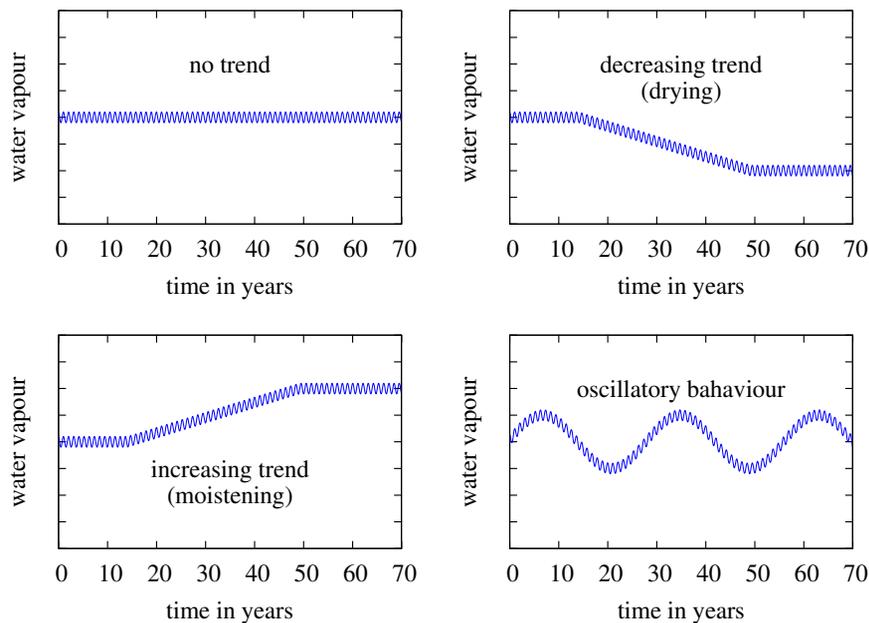
Fig. 2. Schematical evolution of H$_2$O time series: Top left: No trend. Top right: Decreasing trend. Bottom left: Increasing trend. Bottom right: Oscillatory behaviour.

EGU
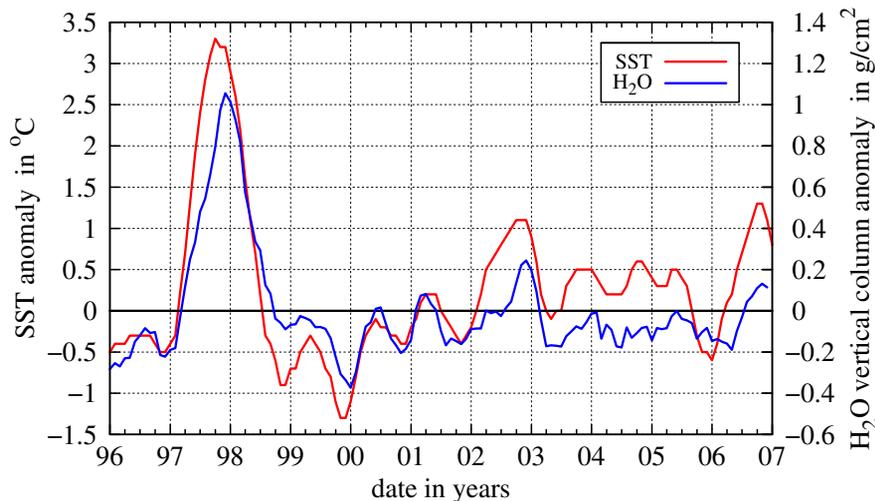
Fig. 3. Monthly mean sea surface temperature (SST) anomalies (red) and GOME/SCIAMACHY H$_2$O total column anomalies (blue) averaged for the area 4° N to 4° S and 150° W to 90° W and both smoothed by a 5 months running mean filter. SST Data taken from http://coaps.fsu.edu/jma.shtml.

H$_2$O vertical column trends 1996–2006 in g/cm^2 per year

H$_2$O vertical column trends 1996–2006 in % per year
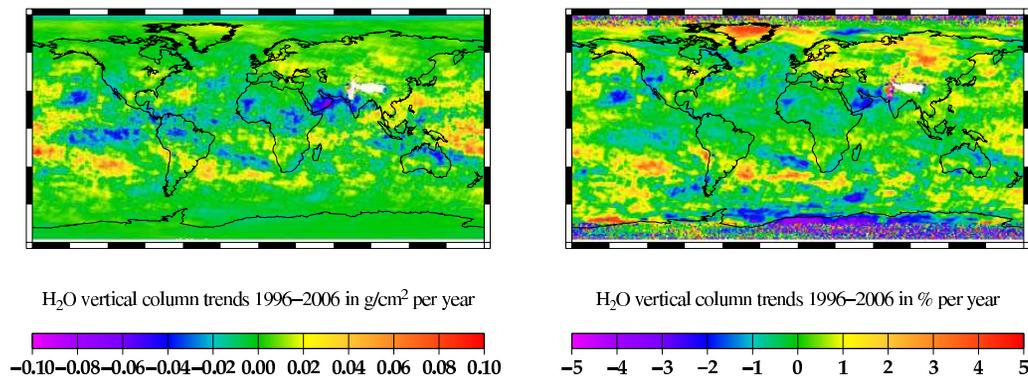
Fig. 4. Left: Absolute H$_2$O trends. Right: Relative H$_2$O trends. (1996 to 2006)

H$_2$O vertical column trends 1996–2006 in g/cm^2 per year

H$_2$O vertical column trends 1996–2006 in % per year

Fig. 5. Left: Absolute significant H$_2$O trends. Right: Relative significant H$_2$O trends. (1996 to 2006)

Title Page

Abstract   Introduction

Conclusions   References

Tables   Figures

I◄   ►I

◄   ►

Back   Close

Full Screen / Esc

Printer-friendly Version

Interactive Discussion

EGU
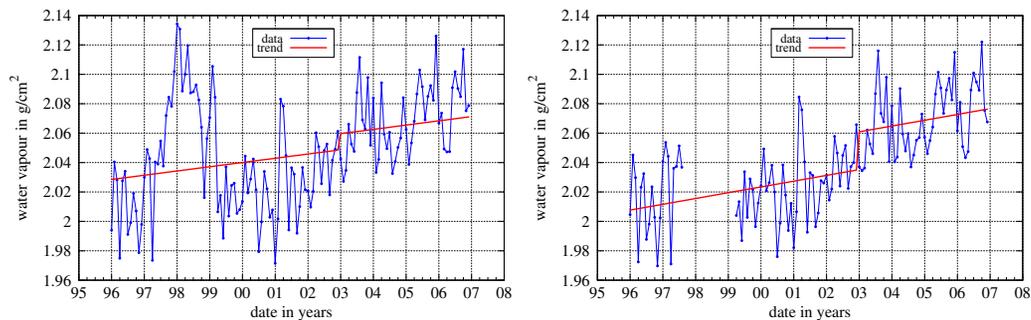
Fig. 6. Two time series of deseasonalised spatially averaged monthly means of the entire globe with the trend (red line) regarding autocorrelations. Left: Including El Niño data. Right: With removed El Niño measurements.

EGU

water vapour in g/cm^2
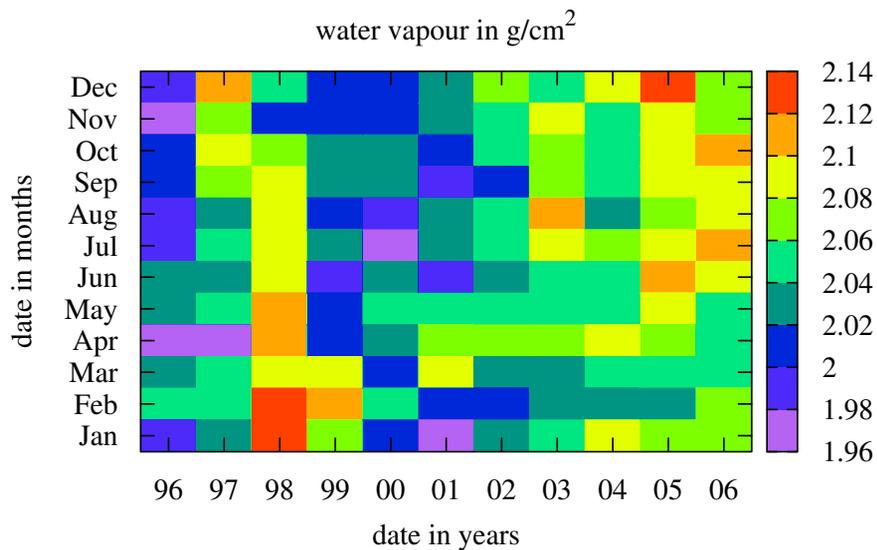
Fig. 7. Time series of months plotted against years, while the deseasonalised globally averaged H$_2$O column amounts are coded with colours.

EGU

EGU
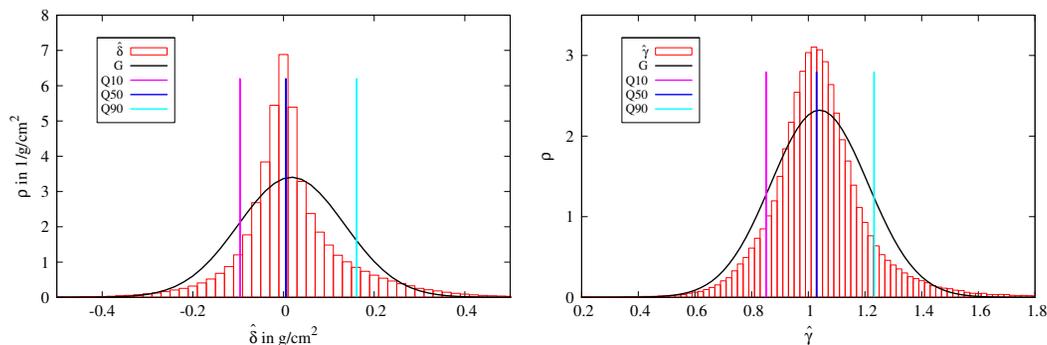
Fig. 8. Left: Density distribution of the mean level shift ($\hat{\delta}$) together with a fitted Gaussian (G), the median (Q50), and the 10 % (Q10) as well as 90 % (Q90) quantiles. Right: Same as left, but here the density distribution of the amplitude changes ($\hat{\gamma}$) between the data before and after the level shift are shown.